NADPH Oxidase NOX2 Defines a New Antagonistic Role for Reactive Oxygen Species and cAMP/PKA in the Regulation of Insulin Secretion

Ning Li,[1] Bin Li,[2] Thierry Brun,[1] Christine Deffert-Delbouille,[2] Zahia Mahiout,[2] Youssef Daali,[3] Xiao-Juan Ma,[2] Karl-Heinz Krause,[2] and Pierre Maechler[1]

In insulin-secreting cells, expression of NADPH oxidase (NOX), a potent source of ROS, has been reported, along with controversial findings regarding its function. Here, the role of NOXs was investigated: first by expression and cellular localization in mouse and human pancreatic islets, and then by functional studies in islets isolated from Nox isoform–specific knockout mice. Both human and mouse β-cells express NOX, in particular NOX2. With use of Nox isoform–specific knockout mice, functional analysis revealed Nox2 as the predominant isoform. In human islets, NOX2 colocalized with both insulin granules and endosome/lysosome membranes. Nox2-deficient islets stimulated with 22.8 mmol/L glucose exhibited potentiation of insulin release compared with controls, an effect confirmed with in vitro knockdown of Nox2. The enhanced secretory function in Nox2-deficient islets was associated with both lower superoxide levels and elevated cAMP concentrations. In control islets, GLP-1 and other cAMP inducers suppressed glucose-induced ROS production similarly to Nox2 deficiency. Inhibiting cAMP-dependent protein kinase reduced the secretory response in Nox2-null islets, although not in control islets. This study ascribes a new role for NOX2 in pancreatic β-cells as negative modulator of the secretory response, reducing cAMP/PKA signaling secondary to ROS generation. Results also show reciprocal inhibition between the cAMP/PKA pathway and ROS. *Diabetes* **61:2842–2850, 2012**

N OX enzymes generate superoxide by transferring one electron from NADPH to oxygen (1). The best known NOX isoform is the phagocyte NADPH oxidase (NOX), a multicomponent complex comprising a membrane catalytic heterodimer, the flavocytochrome b_{558}, formed by $gp91^{phox}$ (also referred to as NOX2) and $p22^{phox}$ (where *phox* is phagocyte oxidase). The cytosolic regulatory subunits are composed of $p40^{phox}$, $p47^{phox}$, $p67^{phox}$, and GTPases Rac1 or Rac2 (1). Assembly of cytosolic elements to membrane catalytic core initiates the activation of NOX. To date, seven isoforms of NOX (NOX1–5 and dual oxidases DUOX1–2) have been identified with different activation mechanisms and heterogeneous tissue distribution (1). In addition to microbial attack by professional phagocytes, physiopathological roles of NOX have recently attracted attention in nonphagocytic cells, including pancreatic β-cells (2–7). Reactive oxygen species (ROS), such as superoxide and hydrogen peroxide, might participate in β-cell dysfunction (8). The redox imbalance favored by high metabolic rate and a relatively low detoxifying system has contributed to the general concept that β-cells are sensitive to ROS, although they can handle rather high concentrations of H_2O_2 (9).

NOX family represents one of the potential sources of ROS in insulin-secreting cells (4). Both rat islets and insulinoma express membrane-associated catalytic components Nox1, Nox2, Nox4, and $p22^{phox}$, as well as cytosolic regulators $p40^{phox}$, $p47^{phox}$, and $p67^{phox}$ and their homologs Noxo1 and Noxa1 (3,5,6). Regarding their putative function in the β-cell, NOXs have been implicated in glucose-induced ROS production in MIN-6 cells (10). Knockdown of $p47^{phox}$ results in total inhibition of glucose-stimulated insulin secretion and lowers ROS (11). In animal models of type 2 diabetes, islets exhibit increased NOX components Nox2 and $p22^{phox}$, correlating with increased oxidative stress (12). Activation of Nox and accompanying ROS generation were demonstrated in Zucker diabetic fatty (ZDF) rat and diabetic human islets (13). However, inhibition of islet NOX using diphenyleneiodonium (DPI) impairs glucose-stimulated insulin secretion (6) along with blunted glucose-induced superoxide production (5,10). These conflicting findings regarding NOX activity and β-cell function might be attributed to poor specificity of old-generation NOX inhibitors, such as apocynin and DPI (14). The former has been shown to function as a general ROS scavenger, and the latter is a nonspecific inhibitor of electron transporters (1,15).

In the current study, we first investigated relative expression levels of the different catalytic subunits of NOXs in both human and mouse pancreatic islets. Then, subcellular distribution of the identified predominant NOX isoform NOX2 was assessed in human islet cells. For avoidance of poor specificity of NOX inhibitors, islets isolated from Nox isoform–specific–deficient mice were used to investigate the contribution of NOXs in insulin secretory function.

RESEARCH DESIGN AND METHODS

Nox2-deficient mice were originally generated by Pollock et al. (16) and were purchased from The Jackson Laboratory (Bar Harbor, MA). We recently generated knockout mice for Nox1 (17) and Nox4 (18). Overall phenotype of Nox2 knockout (Nox2ko) mice is available at www.jax.org under the reference B6.129S-$Cybb^{tm1Din}$/J. Regarding infection susceptibility, there is no evidence for increased infection rate in Nox1- and Nox4-deficient mice, while

Nox2-null mice may exhibit immune defects. In order to avoid potential risks of infectious problems, animals were kept under specific pathogen-free conditions (Centre Médical Universitaire-Zootechnie, Geneva, Switzerland) and systematically examined for signs of skin infection or weight loss during the period preceding the experiments. Knockout animals of 2–4 months of age were age matched with C57BL/6J (wild-type [WT]) control mice. The study was approved by the official ethics committee.

Pancreatic islet isolation and β-cell purification. Mouse pancreatic islets were isolated by collagenase digestion and cultured overnight free floating in RPMI-1640 medium before handpicking for experiments as previously described (19). Freshly isolated human islets from three different donors, who had provided written informed consent, were obtained from D. Bosco and T. Berney (Cell Isolation and Transplantation Center, Department of Surgery, Geneva University Hospital). The use of human islets for research was approved by the institutional ethics committee. Human islets were maintained in CMRL-1066 for 24 h before experiments (20). Mouse pancreatic β-cells were purified by fluorescence-activated cell sorting as previously described (21).

Expression analyses by reverse transcriptase-PCR. Total RNA from 600 mouse islets and 1,200 human islets was extracted using the RNeasy microkit with DNase treatment (Qiagen, Hilden, Germany). First-strand cDNA synthesis was performed with 1 μg RNA, 200 units of reverse transcriptase (SuperScript II Reverse Transcriptase; Invitrogen), and 250 ng random primers (Promega, Madison, WI). PCR was performed at 35 and 40 cycles for each component tested in whole islets and at 40 cycles for Nox2 in sorted mouse β-cells. PCR products were separated in a 1% (w/v) agarose gel stained with ethidium bromide. Details of PCR conditions are summarized in Supplementary Table 1 (mouse) and Supplementary Table 2 (human), with *GAPDH* serving as the housekeeping gene. Quantitative PCR was performed using a StepOnePlus Real-Time PCR system (Applied Biosystems; Life Technologies), and PCR products were quantified fluorometrically using the FastStart Universal SYBR Green Master (ROX; Roche Diagnostics). Negative PCR controls were conducted with RNA without reverse transcriptase (RT) reaction. Details of primers used in quantitative RT-PCR are summarized in Supplementary Table 3. The values obtained were normalized to values of the reference cDNA of cyclophilin.

NOX2 subcellular localization in human islets. Human islets were dispersed at 37°C with 0.05% trypsin-EDTA solution (Invitrogen) for 15 min with regular pipetting before seeding on coverslips precoated with poly-L-ornithine (Sigma-Aldrich) and left for overnight attachment. First, for endosome labeling, islet cells were incubated with 2.5 mg/mL 10 kDa fluorescent fluid-phase marker rhodamine-dextran (Molecular Probes, Eugene, OR) for 15 min at 37°C in culture medium containing 1% FCS and then fixed with 4% paraformaldehyde. For subsequent immunofluorescence, fixed cells were permeabilized with 0.1% Triton X-100 in PBS. Slides were blocked with PBS/3% BSA/0.1% Tween-20 for 30 min before incubation for 2 h with monoclonal mouse antibody against human NOX2 (1:250 dilution; kindly provided by D. Roos, University of Amsterdam, Academic Medical Centre), polyclonal rabbit antibody against human lysosome–associated membrane protein (LAMP)-1 (1:150 dilution; Thermo Scientific), and polyclonal porcine anti–guinea pig insulin (1:400 dilution; DAKO, Carpinteria, CA) antibodies. Specificity of anti-human NOX2 was verified by immunoblotting on extracts of human myeloid leukemia cell lines expressing or not expressing NOX2 (data not shown), showing selective immunoreactivity for both unglycosylated precursor and mature glycoprotein of NOX2. Of note, reliable antibodies against mouse Nox2 are not available. Next, slides were exposed to fluorescent dye–labeled secondary antibodies anti-mouse Alexa Fluor 488, anti-rabbit Alexa Fluor 555, and anti–guinea pig Alexa Fluor 647 (Molecular Probes) for 1 h at 1:500 dilution. Nuclei were visualized by DAPI counterstaining. Images were captured on a Zeiss LSM 510 Meta confocal laser system (Carl Zeiss, Feldbach, Switzerland) equipped with a ×63 Plan-Apochromat oil objective. Tissues incubated without primary antibodies served as negative controls.

Insulin secretion. Prior to the experiments, islets were maintained for 1 h in Krebs-Ringer bicarbonate HEPES (KRBH) buffer containing 0.1% BSA (KRBH/BSA) at 2.8 mmol/L glucose (19). Where indicated, we paralleled glucose-stimulated insulin secretion and superoxide generation on the same islets. Batches of 15 islets were handpicked and incubated for 90 min in the presence of 0.2% nitroblue tetrazolium (Sigma-Aldrich). Then, supernatant was collected for measurements of secreted insulin and islets were collected to determine the amount of superoxide generated as described below. Secretion experiments were also conducted in the absence of nitroblue tetrazolium at 2.8 and 22.8 mmol/L glucose in the presence of cAMP inducers glucagon-like peptide (GLP)-1 (10 nmol/L) or forskolin (10 μmol/L) combined with the phosphodiesterase inhibitor 3-isobutyl-1-methylxanthine (IBMX) (100 μmol/L) as indicated. In addition, we tested DPI, previously used as a NOX inhibitor, added 20 min in advance and during stimulation. H89, inhibitor of cAMP-dependent protein kinase (PKA) (22), was preincubated for 30 min and during stimulation. At the end of incubation periods, supernatant was collected for

insulin measurement and islet pellets were resuspended in acid-ethanol to determine insulin contents by radioimmunoassay (Linco Research, St. Charles, MO).

Superoxide generation. Superoxides were detected by both nitroblue tetrazolium assay (23) and dihydroethidine assay using high-performance liquid chromatography (HPLC) and fluorescence (24). For nitroblue tetrazolium assay, yellow water-soluble nitroblue tetrazolium was reduced to dark-blue water-insoluble formazan by superoxide generated in 15 islets/mL KRBH/BSA buffer with 0.2% nitroblue tetrazolium (23). The samples were incubated for 90 min at 37°C with either basal 2.8 mmol/L or stimulatory 22.8 mmol/L glucose in the presence or absence of cAMP inducers as mentioned above. Islets were centrifuged (13,000 rpm, 5 min, 4°C), the supernatant was discarded, and then cells were broken in 2 mol/L KOH and formazan (nitroblue tetrazolium reduced to insoluble) dissolved in DMSO. Absorbance was determined at 620 nm in a microtiter plate reader (Wallac 1420; Perkin Elmer, Courtaboeuf, France), and data were expressed as optical density per 15 islets.

Superoxide generation was also monitored using dihydroethidine, which becomes fluorescent upon reaction with superoxides (24). After preincubation for 1 h at 2.8 mmol/L glucose in KRBH/BSA, groups of 50 islets were stimulated with 22.8 mmol/L glucose for 30 min before exposure to 50 μmol/L dihydroethidine for 30 min. Then, islets were pelleted down, resuspended in methanol, and homogenized. The homogenate was centrifuged at 13,000 rpm for 5 min, and the supernatant was collected for speed vacuum concentrator and protein measurement before the resulting sample was dissolved in 100 μL bdH$_2$O for HPLC. Dihydroethidine and its two oxidized products, i.e., superoxide-specific 2-hydroxyethidium (EOH) (24) and ethidium, were separated by HPLC equipped with a fluorescence detector with excitation at 510 nm and emission at 595 nm. Area under EOH peak was normalized to proteins.

Glucose tolerance test. Glucose tolerance and insulin levels were recorded on overnight (15 h)-fasted mice injected with glucose (3 mg/g body wt i.p.). Whole blood was collected for glucose level measurements using a glucometer (Roche Diagnostics). Additionally, plasma insulin levels were determined at time 0, 2, 8, and 15 min using an ultrasensitive mouse insulin ELISA (Mercodia, Uppsala, Sweden).

Knockdown of Nox2 in islet cells. Freshly isolated mouse islets were dispersed at 37°C into single cells by addition of 0.05% trypsin-EDTA solution for <5 min with gentle pipetting. The dispersed cells were washed with RPMI-1640 and divided into two equal fractions. Each fraction was placed on poly-L-ornithine–precoated 48-well plates followed by transfection with 100 nmol/L scramble oligos or an equal mixture of four small interfering (si)RNA oligos targeting Nox2 (Supplementary Table 4) (ON-TARGETplus SMARTpool siRNA; Thermo Scientific) using 10 μg/600 μL Lipofectamine 2000 (Invitrogen) in 1% FCS RPMI-1640 medium. After 4 h, the transfection medium was replaced by complete culture medium. The dispersed islet cells were kept in standard culture conditions for 48 h before RNA extraction and insulin secretion assay.

Ca^{2+} measurement. Cellular Ca^{2+} changes were monitored as ratiometric measurements of Fura-2 fluorescence. Isolated mouse islets were cultured on poly-L-lysine (Sigma)-treated glass coverslips that were placed in a thermostatic chamber (Harvard Apparatus) before incubation with 2 μmol/L Fura-2/acetoxymethyl ester (AM) for 60 min. After washing, Fura-2 fluorescence of a single islet was imaged with alternate 340/380 nm excitation and 510 nm emission using an Axiovert S100 TV through a 40 × 1.3 NA oil immersion objective (Carl Zeiss).

Islet cAMP content. Islets in groups of 40 were handpicked and preincubated for 1 h at 2.8 mmol/L glucose in KRBH/BSA before stimulation with 22.8 mmol/L glucose for 1 h. Then, supernatants were removed and islets washed once with ice-cold KRBH, and ice-cold HCl (100 μL at 0.1 mmol/L) was added to islet pellets followed by 10-min agitation at 4°C. After neutralization with 100 μL 0.1 mmol/L NaOH, islet cAMP content was determined using an ELISA kit (Amersham Biosciences) following the manufacturer's instructions.

Statistical analysis. Data are presented as means ± SEM. Differences between the NOX knockouts and the WT controls were analyzed by one-way ANOVA followed by Turkey or least significant difference posttest with IBM SPSS statistics software (version 19) unless otherwise indicated. A P value <0.05 was considered statistically significant.

RESULTS

Expression and cellular localization of NOX in human islet cells. Conventional RT-PCR showed that human islet cells express *NOX* isoforms *NOX2*, *-4*, and *-5* at the mRNA level (Fig. 1*A*). Expression was confirmed by quantitative real-time RT-PCR, giving a cycle threshold (C_T) of 28.9 for *NOX2* and >30 for other isoforms, compatible with higher *NOX2* expression. Immunofluorescence on dispersed

human islet cells revealed the presence of NOX2 in insulin-positive cells (Fig. 1B–E). Intriguingly, NOX2 labeling displayed colocalization with both insulin granule and endosome-like structures. Regarding the latter, two
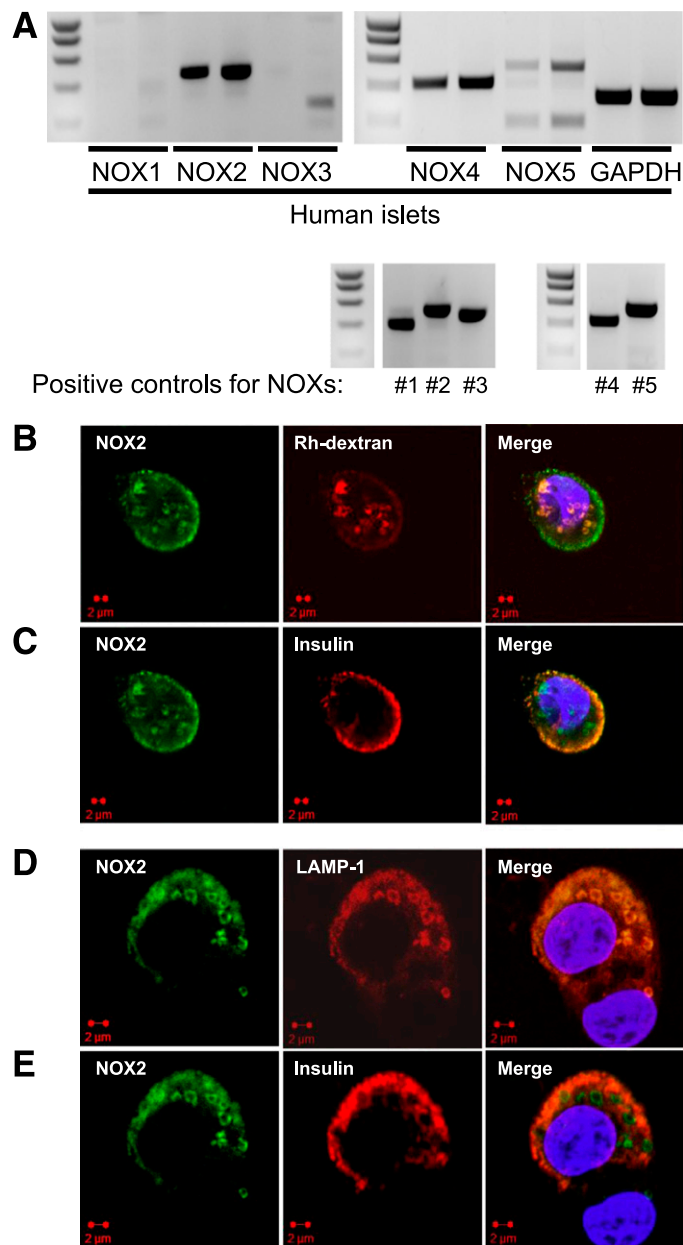
FIG. 1. Gene expression of NOX components and NOX2 localization in human islets. A: Expression of catalytic NOX subunits in human islets (upper panel) was detected at the mRNA level by RT-PCR (for each gene, 35/40 cycles in the left and right lanes, respectively). Positive controls (lower panel) were performed on cDNA from human colon carcinoma cell line Caco-2 for NOX1 (#1), human neutrophils for NOX2 (#2), human embryonic kidney (HEK) cells transduced with human NOX3 gene (HEK-NOX3, #3), human microglia cell line clone 3 (HMC3) for NOX4 (#4), and HEK cells transduced with human NOX5 gene (HEK-NOX5, #5). B–E: Cellular localization by immunofluorescence of NOX2 (green) in β-cells from dissociated human islets combined with detection in red of rhodamine-conjugated dextran (Rh-dextran)-labeled early endosome (B) and insulin (C), late endosome and lysosome marker LAMP-1 (D), and insulin (E). Nuclei were stained in blue with DAPI. Fluorescence staining was performed with three independent batches of human pancreatic islet cells. GAPDH, glyceraldehyde-3-phosphate dehydrogenase. (A high-quality digital representation of this figure is available in the online issue.)

approaches were used to study this specific subcellular localization. First, rhodamine-conjugated dextran (10 kDa), whose internalization and accumulation have been applied to identify the fluid phase of early endosomal structure (25), revealed vesicles of ~1–2 μm in human β-cells. These dextran-positive structures were recognized by antibody against human NOX2 (Fig. 1B). Consistently, pattern of NOX2-containing vesicles was similar to that of late endosome/lysosome marker LAMP-1 (Fig. 1D). Apart from endosomal/lysosomal localization, NOX2 staining was also found in the periphery of β-cells, overlapping with insulin staining (Fig. 1C and E).

Expression of NOX in mouse pancreatic islets. With the exception that NOX5 is exclusively expressed in tissues of human origin (1), expression profile of catalytic Nox enzymes in mouse islets was similar to human islets, with $Nox2$ being the only isoform efficiently amplified after 35 PCR cycles (Fig. 2A). Consistently, quantitative real-time RT-PCR analysis on WT islets revealed C_T values of 29.8 ± 0.9 for $Nox2$, 30.5 ± 0.6 for $Nox4$, and 33.7 ± 0.2 for $Nox1$ compared with 23.3 ± 1.3 for the housekeeping gene $cyclophilin$ ($N = 5$ independent experiments). As negative control, C_T values with versus without reverse transcriptase showed the strongest difference for $Nox2$ ($Nox2$ −RT 35.6 ± 0.2, Δ5.8; $Nox4$ 33.0 ± 0.2, Δ2.5; and $Nox1$ 34.6 ± 0.5, Δ0.9), suggesting relatively high expression of $Nox2$
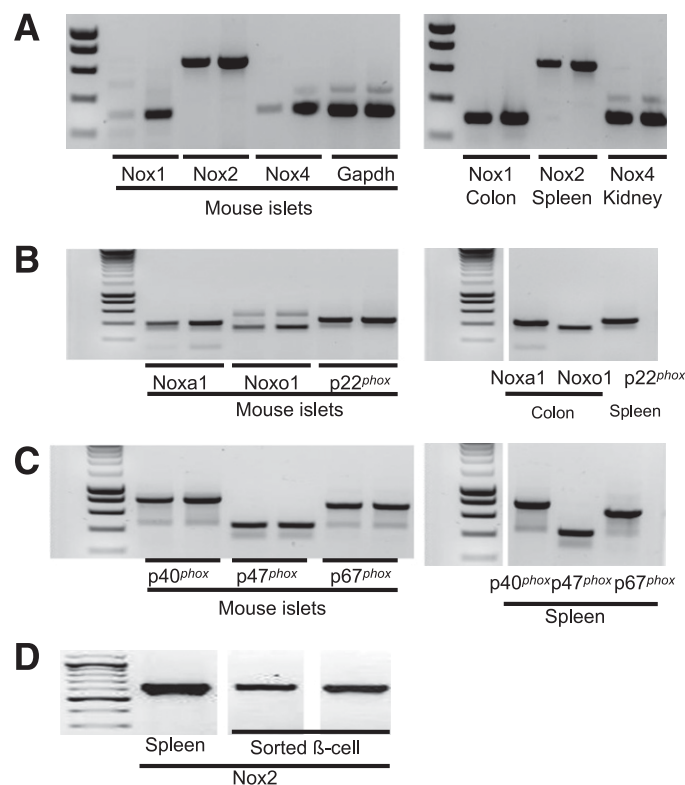

FIG. 2. Gene expression of NOX components in mouse islets and purified β-cells. A, B, and C: Expression of catalytic Nox subunits in mouse islets (left panels of A–C) was detected at the mRNA level by RT-PCR (for each gene, 35 and 40 cycles for the left and right lanes, respectively). Positive controls (right panels of A–C) were performed with cDNA from mouse colon for Nox1, Noxa1 (homolog of p67^{phox}), and Noxo1 (homolog of p47^{phox}); from spleen for Nox2, p22^{phox}, p40^{phox}, p47^{phox}, and p67^{phox}; and from kidney for Nox4. D: Nox2 expression (40 cycles of PCR) in purified β-cells from two C57BL/6J mice with cDNA from mouse spleen as positive control. Gapdh, glyceraldehyde-3-phosphate dehydrogenase.

and near absence of *Nox1*. In Nox2-deficient islets, high 32.4 C_T value was required to get a positive signal, indicative of background unspecific amplification, while no differences in *Nox1* and *Nox4* expression were recorded, arguing against compensatory mechanisms. The mRNA of p22^{phox} and cytosolic elements p40^{phox}, p47^{phox}, and p67^{phox} and their homologs Noxo1 and Noxa1 were all expressed in mouse islets (Fig. 2*B* and *C*). Nox2 expression was specific for β-cells, as confirmed using cDNA obtained from β-cells of mouse islets sorted by fluorescence-activated cell sorter (Fig. 2*D*). Thus, both human and mouse β-cells express NOX, with NOX2 being expressed in both species.

Islet morphology and insulin content of Nox2-deficient mice. No significant differences in the size or organization of islets were observed between WT and Nox2-deficient mice, which exhibited the expected distribution of α and β-cells (Supplementary Fig. 1). Islet insulin contents were similar between WT (25.1 ± 9.8 ng/islet) and Nox2-deficient (22.5 ± 10.3 ng/islet) mice ($N = 4$), indicating that Nox2 may not be involved in the regulation of insulin synthesis.

Nox2 deficiency reduces ROS generation and potentiates the glucose response. For investigation of the role of Nox enzymes in islet function, glucose-stimulated superoxide generation and insulin secretion were simultaneously
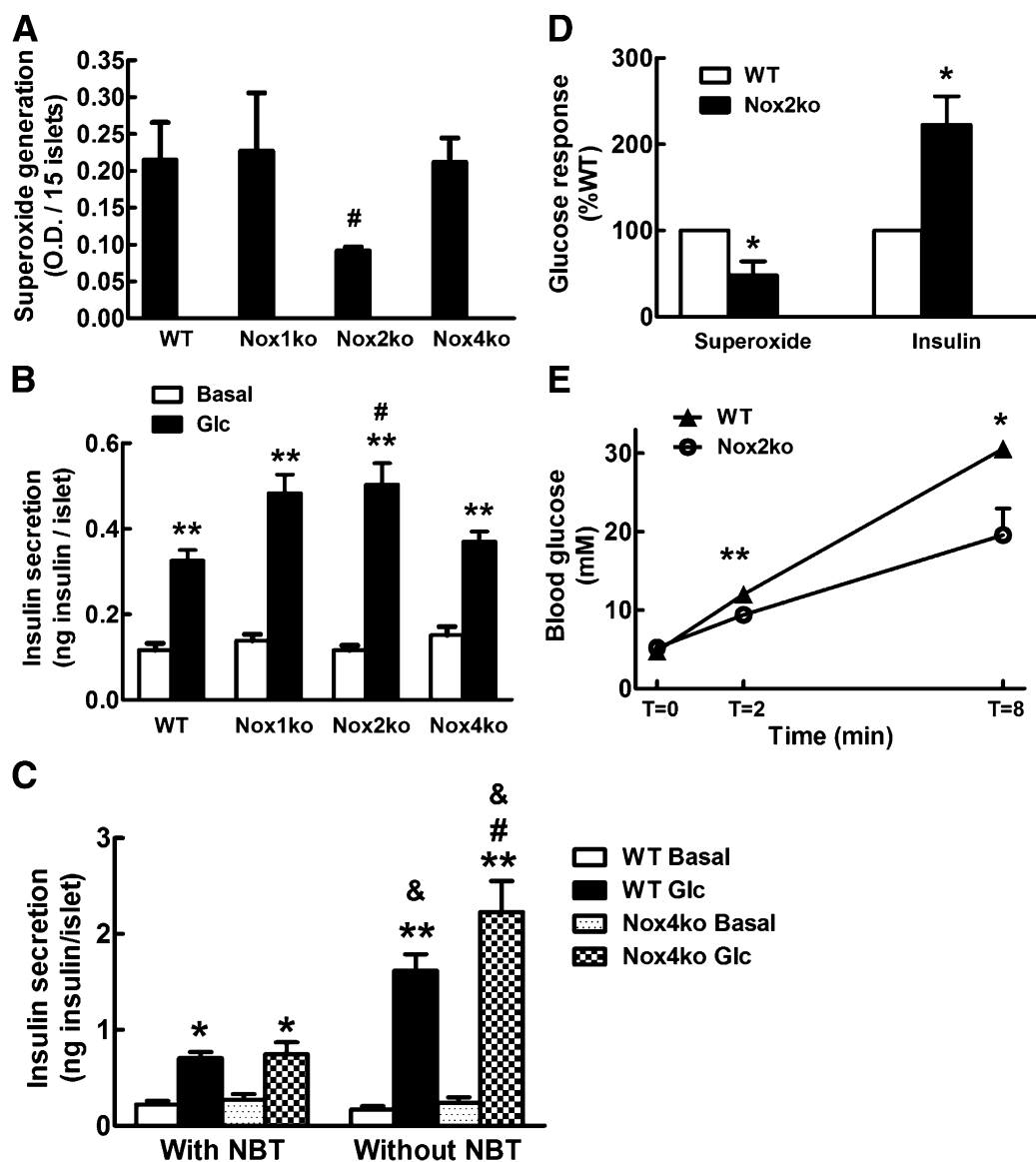
FIG. 3. Glucose (Glc)-induced superoxide generation and insulin secretion in control WT and Nox-deficient islets. *A* and *B*: Glucose-induced superoxide generation (*A*) and insulin secretion (*B*) measured in islets isolated from WT and Nox1ko, Nox2ko, and Nox4ko mice. Islets were incubated at 2.8 mmol/L glucose (basal) or stimulatory 22.8 mmol/L glucose in the presence of nitroblue tetrazolium (NBT) used as a probe for superoxide generation. **$P < 0.01$ vs. corresponding basal of the same genotype; #$P < 0.05$ vs. stimulated WT. *C*: Glucose-stimulated insulin secretion measured on islets isolated from WT and Nox4ko mice in the presence or absence of the superoxide probe nitroblue tetrazolium. *$P < 0.05$, **$P < 0.01$ vs. corresponding basal of the same genotype; #$P < 0.05$ vs. stimulation with 22.8 mmol/L glucose of WT without nitroblue tetrazolium; &$P < 0.05$ vs. corresponding stimulation with 22.8 mmol/L glucose of the same genotype with nitroblue tetrazolium. *D*: Superoxide levels measured by dihydroethidine-based HPLC assay and insulin secretion on WT and Nox2ko islets incubated at 22.8 mmol/L glucose in the absence of nitroblue tetrazolium. *$P < 0.05$ vs. WT. *A–D*: Data are means ± SEM of at least three independent experiments. *E*: In vivo glucose homeostasis in WT and Nox2ko mice. After an overnight fast, WT and Nox2ko mice at 2–3 months of age were subjected to an intraperitoneal glucose tolerance test. Glycemia were determined before ($T = 0$) and at 2 min ($T = 2$) and 8 min ($T = 8$) after glucose administration. Data are means ± SEM of five mice in each genotype. *$P < 0.05$, **$P < 0.01$ vs. WT of corresponding time point. O.D., optical density.

determined in the same islets obtained from WT and Nox1-, Nox2-, and Nox4-deficient mice. In WT islets, nitroblue tetrazolium assay showed that superoxide levels were enhanced 1.9-fold when glucose was raised from 2.8 to 22.8 mmol/L ($P < 0.05$). In Nox2-deficient islets, superoxide levels at 22.8 mmol/L glucose were reduced by 56% compared with WT ($P < 0.05$) (Fig. 3A), whereas no significant changes were recorded in islets of Nox1- and Nox4-deficient mice.

Regarding insulin release in the presence of nitroblue tetrazolium, stimulatory 22.8 mmol/L glucose induced a 2.8-fold secretory response compared with basal 2.8 mmol/L glucose ($P < 0.01$) in WT islets (Fig. 3B). Responses in Nox-deficient islets were 3.5-fold ($P < 0.01$) for Nox1ko, 2.5-fold ($P < 0.01$) for Nox4ko, and 4.4-fold for Nox2ko ($P < 0.01$) mice, with the latter exhibiting significant enhancement of the glucose response compared with WT (+55%, $P < 0.05$) (Fig. 3B). Superoxide levels and secretory responses pointed to Nox2 as the functionally predominant Nox isoform in mouse islets. Previous studies using DPI as Nox inhibitor reported almost absence of glucose-induced insulin release (6,11). Combining specific Nox deficiency and 10 μmol/L DPI exposure (based on a dose response of DPI [Supplementary Fig. 2A]), we observed an overall suppression of islet secretory function in WT and all Nox-deficient isoforms (Supplementary Fig. 2B). Thus, data showing that Nox deficiency exhibited opposite effects compared with DPI treatment suggest Nox-independent inhibition of insulin secretion by DPI.

It was intriguing that the presence of nitroblue tetrazolium during secretion assay blunted the glucose response in WT islets (Fig. 3C), indicating inhibitory properties of nitroblue tetrazolium. We therefore reexamined glucose-induced insulin secretion without nitroblue tetrazolium on islets of mice deficient in Nox2 and Nox4, two isoforms being expressed in both human and mouse islets. Compared with WT islets, which exhibited a 9.4-fold secretory response, glucose-stimulated insulin secretion in Nox2- and Nox4-deficient islets was potentiated in the absence of nitroblue tetrazolium (123 and 38% [Fig. 3D and C, respectively]). The glucose response tested without nitroblue tetrazolium confirmed inhibitory properties of Nox2 and uncovered similar, but much more modest, effects of Nox4.

Superoxide levels at 22.8 mmol/L glucose were further evaluated by dihydroethidine-based HPLC technique. Compared with WT, Nox2-deficient islets exhibited 52% less superoxide-specific EOH signal ($P < 0.05$) (Fig. 3D), in agreement with the nitroblue tetrazolium assay. This effect was also consistent with dihydroethidine-based direct fluorometric assay, showing a 35% reduction of oxidized dihydroethidine in Nox2ko versus control islets ($P < 0.01$) (Supplementary Fig. 3).

In vivo, basal blood glucose levels of Nox2-deficient mice were comparable with those of control animals. However, in the first minutes of a glucose tolerance test, glycemia was lower in Nox2ko mice compared with that in controls (Fig. 3E). Plasma insulin levels remained similar to those in controls (data not shown), an observation that does not rule out putative transient increased insulin signaling in Nox2-deficient mice, according to the fast insulin clearance from the circulation (26). At time 15 min and onward, glycemia and insulin levels were similar between groups (Supplementary Fig. 4).

Knockdown of Nox2 in islet cells by siRNA. The potentiated insulin release observed in Nox2 knockout islets might be a primary effect of Nox2 deficiency, or alternatively, secondary to developmental or metabolic changes induced by Nox2 deletion. To address this point, we carried out in vitro siRNA-mediated Nox2 silencing in primary mouse β-cells. Efficient knockdown (−93%) of Nox2 in dispersed mouse islet cells (Fig. 4A) resulted in a 2.8-fold secretory response ($P < 0.05$) compared with 1.7-fold ($P < 0.05$) insulin secretion in the scramble control condition ($P < 0.05$) (Fig. 4B). This is consistent with data obtained in islets from Nox2-deficient mice.

Second messengers in Nox2-deficient islets. We next addressed at which step Nox2 might interfere with insulin exocytosis by first investigating glucose-induced $[Ca^{2+}]_i$ responses, which have been reported to be inhibited by DPI (11). Similar elevations of $[Ca^{2+}]_i$ were recorded in WT and Nox2-deficient islets in response to 22.8 mmol/L glucose (Fig. 5A), suggesting alternative signals being implicated in the potentiated secretory response. In this context, cAMP triggered our attention because 1) it potentiates glucose-evoked insulin exocytosis and 2) it inhibits NOXs in neutrophils (27). As expected, in WT islets the cAMP inducers GLP-1 as well as forskolin plus IBMX markedly potentiated glucose-stimulated insulin secretion (Fig. 5B). In Nox2-deficient islets, the enhanced secretory response conferred by the lack of Nox2 was not further elevated by the cAMP inducers, reaching similar levels compared with WT islets treated with the same compounds without additive effects (Fig. 5B). These observations suggest a link between cAMP levels and the redox state of the cell. Indeed, when measured in control WT
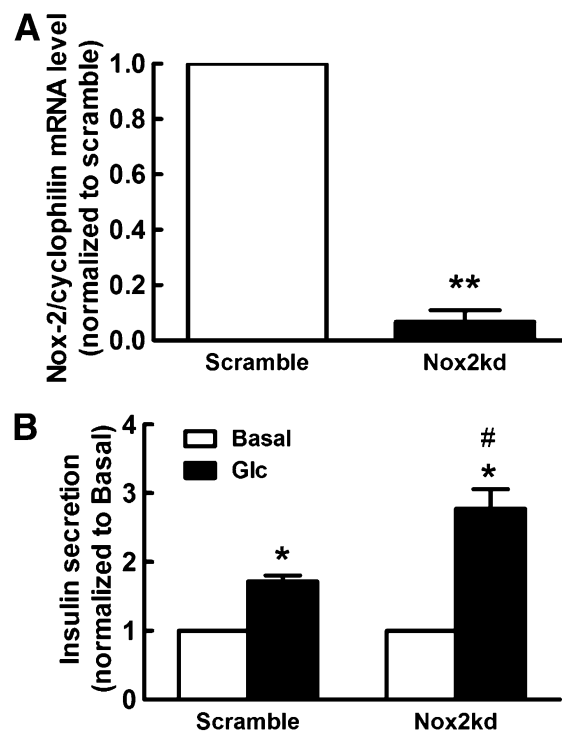
FIG. 4. Knockdown of Nox2 in mouse islet cells and effects on glucose (Glc)-induced insulin secretion. A: The mRNA levels of Nox2 were measured 48 h after scramble siRNA or siNox2 (Nox2kd) transfection of control islet cells. Nox2 mRNA levels are normalized to cyclophilin. **$P < 0.01$ vs. scramble. B: Insulin secretion tested at 2.8 mmol/L glucose (basal) and 22.8 mmol/L glucose on islet cells 48 h after transfection with scramble siRNA or siNox2 (Nox2kd). *$P < 0.05$ vs. corresponding basal condition; #$P < 0.05$ vs. scramble group at 22.8 mmol/L glucose. Data are means ± SEM of three independent experiments.
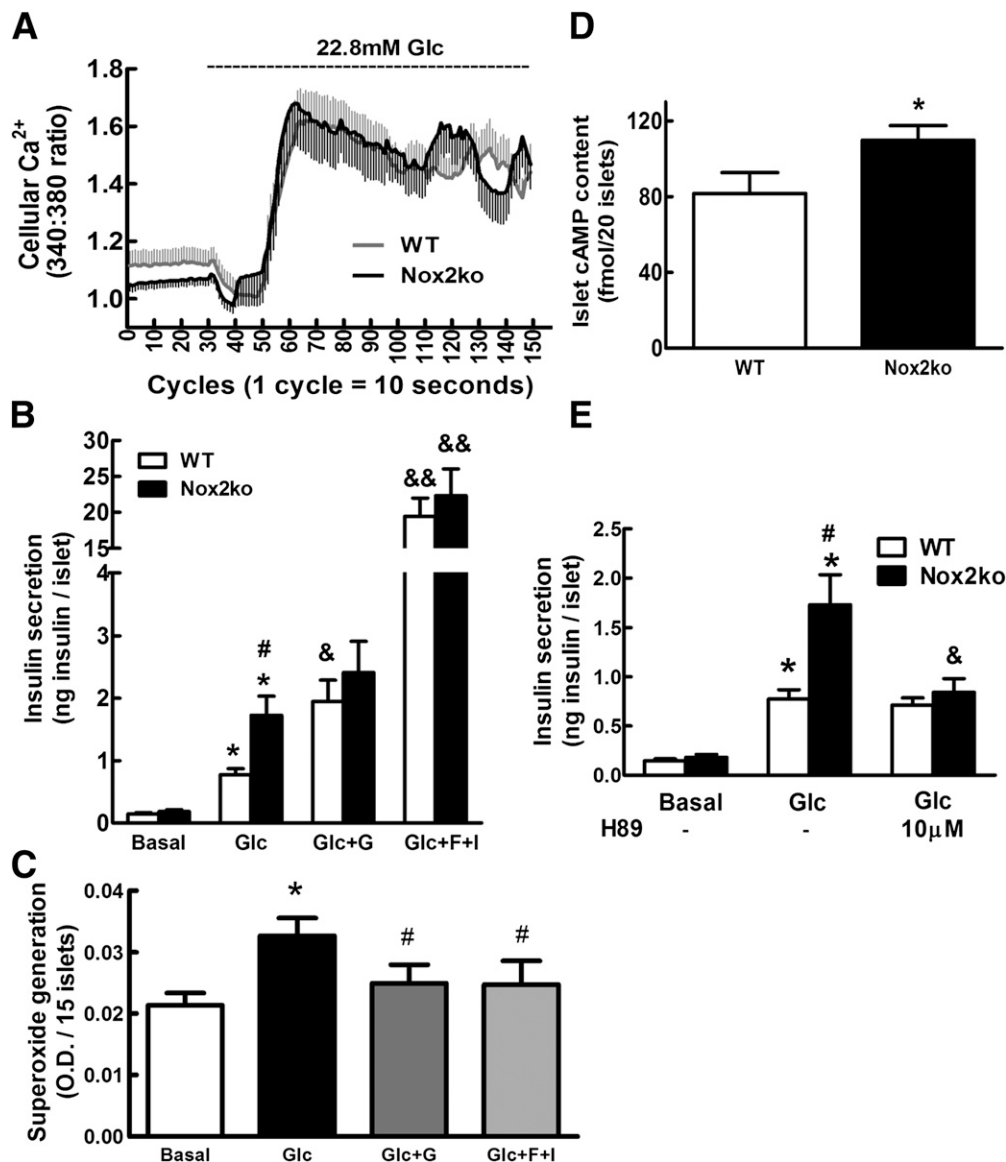
FIG. 5. Cellular Ca^{2+}, insulin secretion, cAMP levels, and ROS generation in Nox2-deficient islets. *A*: Cellular Ca^{2+} levels were measured by Fura-2 fluorescence. Islets were kept at basal 2.8 mmol/L glucose before switching to stimulatory 22.8 mmol/L glucose (Glc). Traces are averages of 11 recordings on islets isolated from four different mice for both control (WT) and Nox2ko mice. *B*: Effects of cAMP inducers on insulin secretion in Nox2-deficient islets compared with responses of WT islets. Conditions include basal release at 2.8 mmol/L glucose (basal), stimulation with 22.8 mmol/L glucose, glucose stimulation in the presence of 10 nmol/L GLP-1 (Glc+G), and glucose stimulation in the presence of 10 μmol/L forskolin plus 100 μmol/L IBMX (Glc+F+I). *P < 0.05 vs. basal condition of the same genotype; &P < 0.05, &&P < 0.01 vs. corresponding stimulation with 22.8 mmol/L glucose condition of the same genotype; #P < 0.05 vs. stimulation with 22.8 mmol/L glucose in WT. *C*: Effects of cAMP inducers 10 nmol/L GLP-1 (G) and 10 μmol/L forskolin plus 100 μmol/L IBMX (F+I) on superoxide generation in control WT islets stimulated with 22.8 mmol/L glucose. *P < 0.05 vs. basal condition; #P < 0.05 vs. stimulation with 22.8 mmol/L glucose condition. *B* and *C*: Data are means ± SEM of four independent experiments. *D*: Islet cAMP content measured after 1 h stimulation with 22.8 mmol/L glucose. *P < 0.05 vs. WT. Data are means ± SEM, WT N = 6, Nox2ko N = 8; statistical analysis by Mann-Whitney U test. *E*: Effect of PKA inhibitor H89 (10 μmol/L) on insulin secretion in WT and Nox2-deficient islets stimulated with 22.8 mmol/L glucose. *P < 0.05 vs. corresponding basal condition of the same genotype; #P < 0.05 vs. corresponding stimulation with 22.8 mmol/L glucose condition of WT, &P < 0.05 vs. stimulation with 22.8 mmol/L glucose condition of the same genotype. Data are means ± SEM of four to six independent experiments. O.D., optical density.

islets, the cAMP inducers suppressed glucose-induced ROS production (P < 0.05) (Fig. 5*C*), which is an effect similar to Nox2 deficiency (Fig. 3*A*). In agreement with these data, cellular cAMP concentrations were found to be higher in Nox2-deficient islets compared with WT after glucose stimulation (34.3%, P < 0.05) (Fig. 5*D*). Overall, data indicate a link between cAMP levels and ROS production, with the lack of the ROS-generator Nox2 preserving cAMP levels and in turn enhancing the secretory response. Elevation of cAMP leads to activation of PKA, which phosphorylates and upregulates components of

exocytosis machinery. In this context, PKA inhibitor H89 (22) was added during glucose stimulation (Fig. 5*E*). H89 had no effect on glucose-induced insulin exocytosis in WT control islets, which is in agreement with a previous study (28). However, in Nox2-deficient islets insulin secretion was reduced by H89, indicating a link between PKA and Nox2.

DISCUSSION

The data demonstrate that both human and mouse β-cells express NOX catalytic subunits, consistent with previous

observations in rat islets (6). Among the different NOXs, NOX2 is functionally the predominant isoform. Regarding subcellular localization, NOX enzymes have been found in membranes of various cell organelles, in relationship with tissue function and the associated NOX activity (29–32). In human β-cells, we observed immune-reactive NOX2 in both endosome/lysosome membranes and insulin granules. The association of NOX2 with insulin-secretory vesicles suggests a redox control of exocytosis as previously described (33). Regarding the presence of NOX2 on late endosome/lysosome membranes, it might reveal the coordinated exocytosis followed by endocytosis of insulin granules as described long ago (34). In human β-cells, residence of NOX2 in a population of vesicles containing endosome/lysosome markers suggests a recruitment of NOX2 from exocytosed secretory vesicles.

Activation of NOX complex requires the assembly of different cytosolic factors, including p47^{phox}, which serves as stabilizer of the complex (35). In rat islets, silencing p47^{phox} by 50% results in total abrogation of glucose-stimulated insulin secretion (11), suggesting implication of other targets. Function of NOXs in pancreatic β-cells has been addressed in previous studies, mostly by use of chemical inhibitors (DPI or apocynin) in an attempt to inhibit NOX, leading to the conclusion that lowering NOX activity impairs insulin secretion (6,36). Here, mouse islets genetically deficient for Nox isoforms did not show any impairment in glucose-stimulated insulin secretion. On the contrary, Nox2-null islets exhibited enhanced secretory responses, while DPI inhibited insulin release in both WT and Nox-deficient islets. DPI, a flavoenzyme inhibitor, interferes not only with Nox activity but also with other flavin-dependent enzymes, such as those required for mitochondrial electron transport chain activity (37), which is mandatory for β-cell function (38). Accordingly, DPI lowers glucose oxidation and intracellular Ca^{2+} signals in rat islets (11), an effect correlating with impaired mitochondrial function (2). Overall, data show that use of DPI might be misleading regarding function of NOXs in β-cells.

To avoid potential off-target NOX inhibition, we used isoform-specific–deficient mice, revealing potentiated glucose-stimulated insulin secretion in islets lacking Nox2 and, to a lesser extent, in Nox4-deficient islets. Deletion of the functionally predominant isoform Nox2 did not induce compensatory upregulation of other Nox catalytic isoforms, which maintained low transcript levels. Although low levels of ROS, possibly generated by mitochondria, have been reported to positively correlate with glucose-stimulated insulin secretion (39), present data argue for an inhibitory effect of Nox-derived ROS on the secretory function. In line with our results, Nox2 deficiency attenuates β-cell destruction and preserves islet function in streptozotocin-induced diabetes, partially through the reduction of ROS generation (7). Additionally, Nox2-derived ROS contribute to dysfunction and apoptosis of NIT-1 β-cells induced by free fatty acids, effects counteracted by the suppression of Nox2 (40). In rats fed a high-fat diet, the adaptative elevated insulin release secondary to peripheral insulin resistance is associated with lower levels of Nox and ROS in their islets (41), raising the question of the phenotype of Nox2 knockouts on an obese background. In a recent study, Nox4 deficiency was shown to render mice more susceptible to diet-induced obesity, along with higher blood insulin levels (42). This phenotype is compatible with the observed increased insulin release from Nox4 knockout islets, although the increase was much less pronounced than that from Nox2 knockout islets (Fig. 3). The potentiated secretory response in islets isolated from Nox2-deficient mice can be considered a direct consequence of Nox2 deficiency, since acute in vitro knockdown of Nox2 resulted in similar effects (Fig. 4).

Previously, the potential role of NOX in the regulation of glucose-induced insulin secretion has been associated with $[Ca^{2+}]_i$, possibly as a result of impaired mitochondrial metabolism with use of DPI, as discussed above. In contrast, Nox2-deficient islets exhibited normal $[Ca^{2+}]_i$ changes indicating alternative signals being implicated. Among them, cAMP is well-known to strongly potentiate the secretory response. Different neurotransmitters and hormones, including glucagon and GLP-1, increase cAMP levels in the β-cell by activating adenylate cyclase (43). Here, the lack of Nox2 pointed to a cAMP/PKA-dependent pathway because Nox2 deletion mimicked GLP-1 effects in terms of both cAMP rise and potentiation of insulin release. Previously, it was shown that PKA inhibition prevents potentiation of insulin secretion induced by a cAMP-raising agent (28). In the current study, inhibition of PKA completely blocked the fraction of enhanced secretory response associated with Nox2 deficiency. Consequently, and according to the absence of $[Ca^{2+}]_i$ changes, implication of PKA-independent mechanisms, such as Epac (44), is unlikely but not impossible. We did not observe additive effects of Nox2 deficiency plus GLP-1 treatment. Therefore, the elevated cAMP levels measured in Nox2-deficient islets, combined with lower ROS, might explain effects on the secretory response, although implication of other signaling molecules cannot be ruled out. On the basis of present and previous data, activation of an adenylate cyclase/cAMP/PKA pathway seems to be redox responsive. At present, there is no evidence for direct interaction of Nox2 with adenylate cyclase. However, both Nox2 (45) and adenylate cyclase (46) have been localized in lipid rafts, suggesting possible cross-talk between these two enzymes. In stimulated neutrophils, cAMP has been proposed as a physiological suppressor of superoxide production (27). Likewise, we observed much lower glucose-induced superoxide production when WT islets were incubated with adenylate cyclase activators. Thus, such a pathway may exert ROS scavenging properties, possibly through protein kinase activation. Recent studies in vascular experimental systems have highlighted adenylate cyclase/cAMP/PKA signaling in the regulation of ROS production, showing inverse correlation between cAMP and ROS levels mediated by adenylate cyclase and PKA (47,48).

Overall, data indicate that in β-cells the adenylate cyclase/cAMP/PKA pathway modulates redox homeostasis and vice versa, since this pathway is in turn redox sensitive. Indeed, oxidants can regulate adenylate cyclase, thereby altering cAMP availability (49), and site-specific oxidation of PKA inhibits its catalytic activity (50). In β-cells, lowering of ROS production would preserve adenylate cyclase activity and cAMP molecules, in turn activating PKA and increasing the secretory response (Fig. 6).

In conclusion, we propose a new role for NOXs in pancreatic β-cells as negative modulators of the secretory response through ROS generation, in turn reducing adenylate cyclase/cAMP/PKA signaling. Thus, the reduced secretory response associated with ROS production would
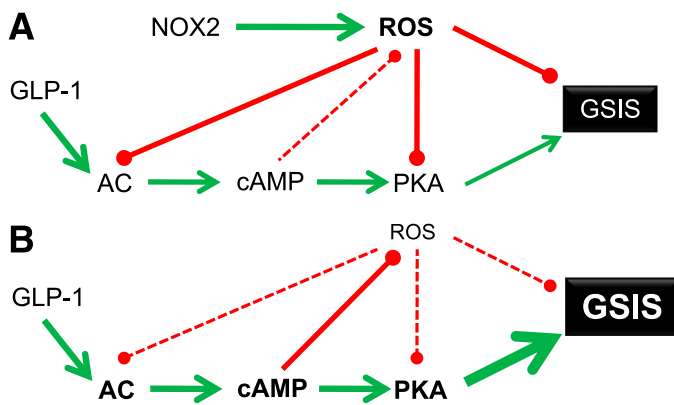
FIG. 6. Proposed model for interactions between ROS and the cAMP/PKA pathway in relationship with glucose-stimulated insulin secretion (GSIS). *A*: In control β-cells, Nox2 generates ROS, which act as negative modulators of glucose-stimulated insulin secretion. GLP-1 induces production of cAMP via ROS-sensitive adenylate cyclase (AC) and reduces ROS effects through cAMP action. ROS may also inhibit PKA activity by residue-specific oxidation, concurring with negative regulation of glucose-stimulated insulin secretion. *B*: In Nox2-deficient β-cells, ROS-mediated inhibitions of glucose-stimulated insulin secretion and adenylate cyclase plus PKA are reduced. Moreover, cAMP molecules are preserved owing to lower ROS production, further reduced by elevated cAMP, resulting in stronger PKA activation and ultimately potentiation of glucose-stimulated insulin secretion.

be contributed by changes in cAMP levels, the most powerful amplifying signal of insulin exocytosis.

ACKNOWLEDGMENTS

REFERENCES

1. Bedard K, Krause KH. The NOX family of ROS-generating NADPH oxidases: physiology and pathophysiology. Physiol Rev 2007;87:245–313

2. Imoto H, Sasaki N, Iwase M, et al. Impaired insulin secretion by diphenyleneiodium associated with perturbation of cytosolic Ca2+ dynamics in pancreatic beta-cells. Endocrinology 2008;149:5391–5400

3. Morgan D, Oliveira-Emilio HR, Keane D, et al. Glucose, palmitate and proinflammatory cytokines modulate production and activity of a phagocyte-like

4. Newsholme P, Morgan D, Rebelato E, et al. Insights into the critical role of NADPH oxidase(s) in the normal and dysregulated pancreatic beta cell. Diabetologia 2009;52:2489–2498

5. Oliveira HR, Verlengia R, Carvalho CR, Britto LR, Curi R, Carpinelli AR. Pancreatic beta-cells express phagocyte-like NAD(P)H oxidase. Diabetes 2003;52:1457–1463

6. Uchizono Y, Takeya R, Iwase M, et al. Expression of isoforms of NADPH oxidase components in rat pancreatic islets. Life Sci 2006;80:133–139

7. Xiang FL, Lu X, Strutt B, Hill DJ, Feng Q. NOX2 deficiency protects against streptozotocin-induced beta-cell destruction and development of diabetes in mice. Diabetes 2010;59:2603–2611

8. Li N, Frigerio F, Maechler P. The sensitivity of pancreatic beta-cells to mitochondrial injuries triggered by lipotoxicity and oxidative stress. Biochem Soc Trans 2008;36:930–934

9. Li N, Brun T, Cnop M, Cunha DA, Eizirik DL, Maechler P. Transient oxidative stress damages mitochondrial machinery inducing persistent beta-cell dysfunction. J Biol Chem 2009;284:23602–23612

10. Tsubouchi H, Inoguchi T, Inuo M, et al. Sulfonylurea as well as elevated glucose levels stimulate reactive oxygen species production in the pancreatic beta-cell line, MIN6-a role of NAD(P)H oxidase in beta-cells. Biochem Biophys Res Commun 2005;326:60–65

11. Morgan D, Rebelato E, Abdulkader F, et al. Association of NAD(P)H oxidase with glucose-induced insulin secretion by pancreatic beta-cells. Endocrinology 2009;150:2197–2201

12. Nakayama M, Inoguchi T, Sonta T, et al. Increased expression of NAD(P)H oxidase in islets of animal models of Type 2 diabetes and its improvement by an AT1 receptor antagonist. Biochem Biophys Res Commun 2005;332:927–933

13. Syed I, Kyathanahalli CN, Jayaram B, et al. Increased phagocyte-like NADPH oxidase and ROS generation in type 2 diabetic ZDF rat and human islets: role of Rac1-JNK1/2 signaling pathway in mitochondrial dysregulation in the diabetic islet. Diabetes 2011;60:2843–2852

14. Jaquet V, Scapozza L, Clark RA, Krause KH, Lambeth JD. Small-molecule NOX inhibitors: ROS-generating NADPH oxidases as therapeutic targets. Antioxid Redox Signal 2009;11:2535–2552

15. Holland PC, Clark MG, Bloxham DP, Lardy HA. Mechanism of action of the hypoglycemic agent diphenyleneiodonium. J Biol Chem 1973;248:6050–6056

16. Pollock JD, Williams DA, Gifford MA, et al. Mouse model of X-linked chronic granulomatous disease, an inherited defect in phagocyte superoxide production. Nat Genet 1995;9:202–209

17. Gavazzi G, Banfi B, Deffert C, et al. Decreased blood pressure in NOX1-deficient mice. FEBS Lett 2006;580:497–504

18. Carnesecchi S, Deffert C, Donati Y, et al. A key role for NOX4 in epithelial cell death during development of lung fibrosis. Antioxid Redox Signal 2011;15:607–619

19. Carobbio S, Ishihara H, Fernandez-Pascual S, Bartley C, Martin-Del-Rio R, Maechler P. Insulin secretion profiles are modified by overexpression of glutamate dehydrogenase in pancreatic islets. Diabetologia 2004;47:266–276

20. Vetterli L, Brun T, Giovannoni L, Bosco D, Maechler P. Resveratrol potentiates glucose-stimulated insulin secretion in INS-1E beta-cells and human islets through a SIRT1-dependent mechanism. J Biol Chem 2011;286:6049–6060

21. Rouiller DG, Cirulli V, Halban PA. Differences in aggregation properties and levels of the neural cell adhesion molecule (NCAM) between islet cell types. Exp Cell Res 1990;191:305–312

22. Nakazaki M, Crane A, Hu M, et al. cAMP-activated protein kinase-independent potentiation of insulin secretion by cAMP is impaired in SUR1 null islets. Diabetes 2002;51:3440–3449

23. Schrenzel J, Serrander L, Bánfi B, et al. Electron currents generated by the human phagocyte NADPH oxidase. Nature 1998;392:734–737

24. Zhao H, Kalivendi S, Zhang H, et al. Superoxide reacts with hydroethidine but forms a fluorescent product that is distinctly different from ethidium: potential implications in intracellular fluorescence detection of superoxide. Free Radic Biol Med 2003;34:1359–1368

25. Alcon-LePoder S, Drouet MT, Roux P, et al. The secreted form of dengue virus nonstructural protein NS1 is endocytosed by hepatocytes and accumulates in late endosomes: implications for viral infectivity. J Virol 2005;79:11403–11411

26. Koschorreck M, Gilles ED. Mathematical modeling and analysis of insulin clearance in vivo. BMC Syst Biol 2008;2:43

27. Bengis-Garber C, Gruener N. Protein kinase A downregulates the phosphorylation of p47 phox in human neutrophils: a possible pathway for inhibition of the respiratory burst. Cell Signal 1996;8:291–296

28. Thams P, Anwar MR, Capito K. Glucose triggers protein kinase A-dependent insulin secretion in mouse pancreatic islets through activation of the K+ATP channel-dependent pathway. Eur J Endocrinol 2005;152:671–677

29. Van Buul JD, Fernandez-Borja M, Anthony EC, Hordijk PL. Expression and localization of NOX2 and NOX4 in primary human endothelial cells. Antioxid Redox Signal 2005;7:308–317

30. Hilenski LL, Clempus RE, Quinn MT, Lambeth JD, Griendling KK. Distinct subcellular localizations of Nox1 and Nox4 in vascular smooth muscle cells. Arterioscler Thromb Vasc Biol 2004;24:677–683

31. Block K, Gorin Y, Abboud HE. Subcellular localization of Nox4 and regulation in diabetes. Proc Natl Acad Sci USA 2009;106:14385–14390

32. Casbon AJ, Allen LA, Dunn KW, Dinauer MC. Macrophage NADPH oxidase flavocytochrome B localizes to the plasma membrane and Rab11-positive recycling endosomes. J Immunol 2009;182:2325–2339

33. Ivarsson R, Quintens R, Dejonghe S, et al. Redox control of exocytosis: regulatory role of NADPH, thioredoxin, and glutaredoxin. Diabetes 2005;54:2132–2142

34. Orci L. A portrait of the pancreatic B-cell. The Minkowski Award Lecture delivered on July 19, 1973, during the 8th Congress of the International Diabetes Federation, held in Brussels, Belgium. Diabetologia 1974;10:163–187

35. Dang PM, Cross AR, Quinn MT, Babior BM. Assembly of the neutrophil respiratory burst oxidase: a direct interaction between p67PHOX and cytochrome b558 II. Proc Natl Acad Sci USA 2002;99:4262–4265

36. Graciano MF, Santos LR, Curi R, Carpinelli AR. NAD(P)H oxidase participates in the palmitate-induced superoxide production and insulin secretion by rat pancreatic islets. J Cell Physiol 2011;226:1110–1117

37. Ragan CI, Bloxham DP. Specific labelling of a constituent polypeptide of bovine heart mitochondrial reduced nicotinamide-adenine dinucleotide-ubiquinone reductase by the inhibitor diphenyleneiodonium. Biochem J 1977;163:605–615

38. Maechler P, Li N, Casimir M, Vetterli L, Frigerio F, Brun T. Role of mitochondria in beta-cell function and dysfunction. Adv Exp Med Biol 2010;654:193–216

39. Pi J, Bai Y, Zhang Q, et al. Reactive oxygen species as a signal in glucose-stimulated insulin secretion. Diabetes 2007;56:1783–1791

40. Yuan H, Zhang X, Huang X, et al. NADPH oxidase 2-derived reactive oxygen species mediate FFAs-induced dysfunction and apoptosis of β-cells via JNK, p38 MAPK and p53 pathways. PLoS ONE 2010;5:e15726

41. Valle MM, Graciano MF, Lopes de Oliveira ER, et al. Alterations of NADPH oxidase activity in rat pancreatic islets induced by a high-fat diet. Pancreas 2011;40:390–395

42. Li Y, Mouche S, Sajic T, et al. Deficiency in the NADPH oxidase 4 predisposes towards diet-induced obesity. Int J Obes (Lond) 20 March 2012. doi: 10.1038/ijo.2011.279. [Epub ahead of print]

43. Schuit FC, Huypens P, Heimberg H, Pipeleers DG. Glucose sensing in pancreatic beta-cells: a model for the study of other glucose-regulated cells in gut, pancreas, and hypothalamus. Diabetes 2001;50:1–11

44. Holz GG. Epac: A new cAMP-binding protein in support of glucagon-like peptide-1 receptor-mediated signal transduction in the pancreatic beta-cell. Diabetes 2004;53:5–13

45. Vilhardt F, van Deurs B. The phagocyte NADPH oxidase depends on cholesterol-enriched membrane microdomains for assembly. EMBO J 2004;23:739–748

46. Cooper DM, Crossthwaite AJ. Higher-order organization and regulation of adenylyl cyclases. Trends Pharmacol Sci 2006;27:426–431

47. Ouchi N, Kihara S, Arita Y, et al. Adiponectin, an adipocyte-derived plasma protein, inhibits endothelial NF-kappaB signaling through a cAMP-dependent pathway. Circulation 2000;102:1296–1301

48. Ouedraogo R, Wu X, Xu SQ, et al. Adiponectin suppression of high-glucose-induced reactive oxygen species in vascular endothelial cells: evidence for involvement of a cAMP signaling pathway. Diabetes 2006;55:1840–1846

49. Persad S, Elimban V, Kaila J, Dhalla NS. Biphasic alterations in cardiac beta-adrenoceptor signal transduction mechanism due to oxyradicals. J Pharmacol Exp Ther 1997;282:1623–1631

50. Humphries KM, Pennypacker JK, Taylor SS. Redox regulation of cAMP-dependent protein kinase signaling: kinase versus phosphatase inactivation. J Biol Chem 2007;282:22072–22079